*Journal of Sound and Vibration* (2002) **249**(3), 429–445
doi:10.1006/jsvi.2001.3870, available online at http://www.idealibrary.com on IDEAL®

# ANALYSIS OF THE RESPONSE OF A CRACKED JEFFCOTT ROTOR TO AXIAL EXCITATION

A. K. Darpe, A. Chawla and K. Gupta

*Department of Mechanical Engineering, Indian Institute of Technology, Hauz Khas, Delhi* 110016, *India. E-mail: kgupta@mech.iitd.ernet.in*

(*Received* 11 *April* 2000, *and in final form* 6 *April* 2001)

The coupling of lateral and longitudinal vibrations due to the presence of transverse surface crack in a rotor is explored. Steady state unbalance response of a Jeffcott rotor with a single centrally situated crack subjected to periodic axial impulses is studied. Partial opening of crack is considered and the stress intensity factor at the crack tip is used to decide the extent of crack opening. A crack in a rotor is known to introduce coupling between lateral and longitudinal vibrations. Therefore, lateral vibration response of a cracked rotor to axial impulses is studied in detail. Spectral analysis of response to periodic multiple axial impulses shows the presence of rotor bending natural frequency as well as side bands around impulse excitation frequency and its harmonics due to modulations caused by rotor running frequency. It is concluded that the above approach can prove to be a useful tool in detecting cracks in rotors.



## 1. INTRODUCTION

Fatigue cracks are a potential source of catastrophic failures in rotors. Researchers have put in considerable effort to develop a foolproof and reliable strategy to detect cracks in rotors. One of the approaches investigated in detail is the phase and amplitude variation in the $2\times$ component of steady state (unbalance) response. Several authors [1–7] have focused their attention on $1\times$ and $2\times$ components of rotor vibration and discussed the effect of crack on these frequency components. Experience, however, has shown that even for shallow to moderate cracks, the presence of $2\times$ component of vibration cannot be considered as a reliable indicator of the presence of a crack in the rotor since there are several other mechanisms in rotor that generate second harmonic ($2\times$) component.

A recent approach to this problem has been to study the coupling between lateral, axial and torsional vibrations caused by the presence of crack in a rotor. Papadopoulos and Dimarogonas [8] studied coupling of bending and torsional vibrations of cracked Timoshenko shaft with an open crack assumption. The presence of bending vibration frequencies in torsional spectra had been cited as potential crack indicators. Muszynska *et al.* [9] analyzed torsional/lateral cross-coupled vibration response. Ostachowicz and Krawczuk [10] analyzed coupled torsional and bending vibrations of a rotor with an open crack using finite element model. They applied an external torsional moment to the rotor and found the effect on lateral vibrations due to coupling effect of crack. Papadopoulos and Dimarogonas [11] studied coupling of lateral and longitudinal vibrations and have proposed the coexistence of lateral and longitudinal vibration frequencies in the same spectrum as an unambiguous crack indicator. They have shown that there exists instability

0022-460X/02/030429 + 17 $35.00/0 

between forward and backward critical speeds as well as at critical speed corresponding to the longitudinal eigenvalue of the shaft.

Papadopoulos and Dimarogonas [12] have observed strong coupling of longitudinal and lateral vibrations and of lateral and torsional vibrations even for relative crack depths of 6% using sweep excitation. They used clamped–free Timoshenko shaft with an open crack model. Papadopoulos and Dimarogonas [13] have studied the stability of cracked shaft in coupled vibration mode. The effect of closing crack was taken into account by representing variation in stiffness in the form of a truncated cosine series. They have reported a case study on 300 MW steam turbine, wherein the lateral vibration spectrum showed subharmonics of fundamental longitudinal natural frequency. They also experimentally verified this coupling phenomenon [14] by using sweep excitation to a clamped shaft.

Iwatsubo *et al.* [15] used external excitation technique and applied it to the cracked shaft but did not consider coupling of vibrations. They used lateral periodic and impact excitation and analyzed lateral response of the cracked rotor. They suggested the presence of combination harmonics due to interaction between impact force and rotation of shaft as the crack indicators. Collins *et al.* [16] studied the detection of cracks using axial impulses to a rotating Timoshenko shaft. They also reported the presence of combination harmonics in the lateral vibration spectrum. The rotor speed considered was above $\frac{1}{2}$ the critical speed and the amplitude of running frequency was dominant in comparison to the sum and difference frequency components.

In this paper, response of a Jeffcott rotor with a centrally situated transverse surface crack subjected to external excitation is analyzed. External excitation is in the form of periodic axial impulses. If the axial vibration frequencies coexist with lateral vibration frequencies in the lateral vibration spectrum, it would confirm the existence of coupling of vibrations in the rotor, which in absence of any other coupling mechanisms, is an indicator of the presence of crack.

The application of compressive axial impulses to the rotor causes high-frequency axial vibrations. The overall state of stress on the crack edge due to the transverse and axial forces decides the status of crack (open or close). In the present work, authors have extended the breathing crack modelling of Jun *et al.* [6, 17] to include the axial co-ordinate. The opening and closing of crack is governed by the status of stress intensity factor along the crack edge. Thus, partially opened crack is also taken into account. Coupled equations of motion involving longitudinal displacement and two (vertical and horizontal) lateral displacements are considered. The response to single and multiple impulses per rotation are computed by numerically integrating the equations of motion using Runge–Kutta method. Frequency spectra of vertical and horizontal lateral rotor vibrations are studied in detail.

## 2. EQUATIONS OF MOTION ACCOUNTING FOR COUPLING BETWEEN LATERAL AND LONGITUDINAL MOTION

Consider a massless elastic shaft of diameter $D$ and length $L$ with a disc of mass $m$ mounted at mid-span. The co-ordinates $y$, $z$ and $\xi$, $\eta$ represent the stationary and rotating axes, respectively, as shown in Figure 1. The co-ordinate $u$ represents longitudinal axis. The eccentricity of the centre of the disc mass $m$ from the geometric centre of the disc is $\varepsilon$ and $\beta$ is the orientation of the eccentricity in the direction of the shaft rotation from $\xi$-axis. $\theta(t)$ is the instantaneous angle of rotation and $\omega$ is the rotational speed. The damping coefficient is $c$.

Considering direct stiffnesses $k_\xi$, $k_\eta$ and $k_u$ in the $\xi$, $\eta$ and $u$ directions, and cross-coupled stiffnesses $k_{\xi\eta}$, $k_{\eta\xi}$, $k_{\xi u}$, $k_{\eta u}$, $k_{u\xi}$, and $k_{u\eta}$ which come into play due to partial opening of the

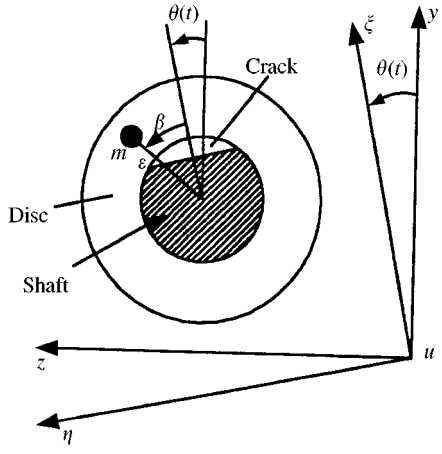


Figure 1. Co-ordinate system.

crack, the equations of motion can be expressed in the rotating co-ordinates as [18]

$$m(\ddot{\xi} - 2\omega\dot{\eta} - \omega^2\xi) + c(\ddot{\xi} - \omega\eta) + k_{\xi}\xi + k_{\xi\eta}\eta + k_{\xi u}u = m\varepsilon\omega^2\cos\beta - mg\cos\theta,$$

$$m(\ddot{\eta} + 2\omega\dot{\xi} - \omega^2\eta) + c(\dot{\eta} + \omega\xi) + k_{\eta\xi}\xi + k_{\eta}\eta + k_{\eta u}u = m\varepsilon\omega^2\sin\beta + mg\sin\theta,$$

$$m\ddot{u} + c\dot{u} + k_{u\xi}\xi + k_{u\eta\eta} + k_u u = 0. \tag{1}$$

Stiffnesses in the equations of motion (1) are response dependent, resulting in non-linear differential equations. In previous literature [2] for steady state response, it has been a usual practice to represent the stiffness variation due to crack breathing during rotation of a cracked rotor by a harmonic function of rotor rotation. This makes the stiffness dependent on rotor angular position and hence, dependent on time. The equations thus become linear. The other more appropriate approach is to use the sign of rotor fixed displacement co-ordinate $\xi$ (Figure 1) to decide the rotor curvature that indicates whether the crack is open or closed and thereby causing the equations to have bi-level stiffnesses. The equations are still response dependent. However, most of the approaches previously used to model the crack work well with gravitational and unbalance excitation at steady state operating speed. They cannot be used in the case of external axial impulses as the crack status in this case depends neither on rotor rotation nor on the sign of $\xi$. The application of compressive axial impulses causes high-frequency axial vibrations and the overall stress on the crack edge due to the transverse forces $Q_{\xi}$, $Q_{\eta}$ and axial force $Q_u$ (Figure 2) decides the status of crack. Hence in the present work, the breathing crack model of Jun *et al.* [6, 17] has been extended to include the axial co-ordinate.

The stiffness depends on the amount of crack opening and the same can be estimated from the stress field along the crack tip. Negative stress intensity factor (SIF) indicates compressive stress field and the crack is closed at that point along the crack tip, whereas positive SIF indicates tensile stress field and the crack in the open state. The SIF is estimated with the assumption of pure bending and no shear deformation. The breathing crack model uses the sign of SIF along the crack edge to decide the amount of closure of crack and thereby estimates the stiffness values to be used in the equations of motion.

Referring to Figure 2, the forces $Q_{\xi}$, $Q_{\eta}$ and $Q_u$ acting on the shaft contribute together to the total stress field along the crack edge. The stress intensity factor, which is indicative of

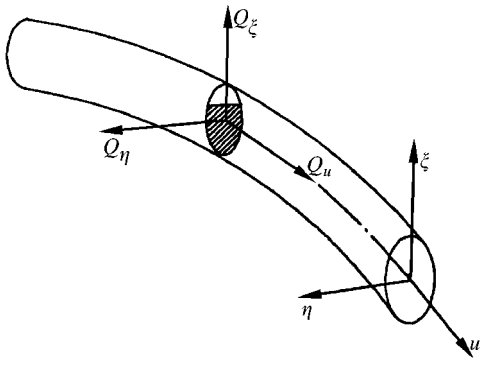


Figure 2. Forces acting on the cross-section containing a crack.

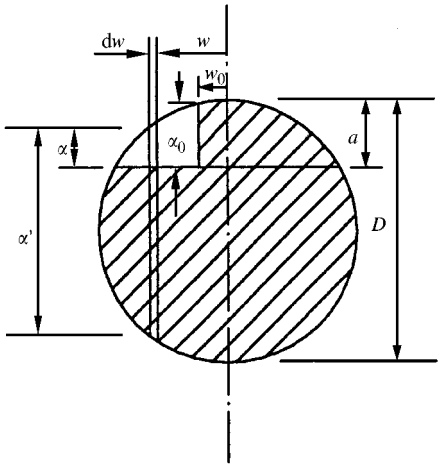


Figure 3. Cross-section containing a crack [6].

the magnitude of this stress field, varies along the crack edge and hence is a function of $w$ (Figure 3). The total stress intensity factor $K^I$ [6, 11, 19] is expressed as follows:

$$K^I = K^I_{Q_\xi} + K^I_{Q_\eta} + K^I_{Q_u}. \tag{2}$$

Here,

$$\begin{aligned} K^I_{Q_\xi} &= \sigma_\xi \sqrt{\pi\alpha} F(\alpha/\alpha'), \\ K^I_{Q_\eta} &= \sigma_\eta \sqrt{\pi\alpha} F'(\alpha/\alpha'), \\ K^I_{Q_u} &= \sigma_u F'(\alpha/\alpha'), \end{aligned} \tag{3}$$

are the SIF due to $Q_\xi$, $Q_\eta$ and $Q_u$, respectively. Here, $\sigma_\xi$ and $\sigma_\eta$ are the bending stresses due to $Q_\xi$ and $Q_\eta$, respectively, and $\sigma_u$ is the axial stress due to $\dot{Q}_u$. These are given by

$$\sigma_\xi(w) = \frac{(Q_\xi L/4)(\alpha'/2)}{I}, \sigma_\eta(w) = \frac{(Q_\eta L/4)w}{I}, \sigma_u = \frac{Q_u}{A},$$

where

$$I = \left(\frac{\pi}{64} D^4\right) \text{ and } A = \left(\frac{\pi}{4} D^2\right). \tag{4}$$

The functions $F$ and $F'$ are given by

$$F(\alpha/\alpha') = \sqrt{\frac{2\alpha'}{\pi\alpha} \tan\left(\frac{\pi\alpha}{2\alpha'}\right)} \frac{0{\cdot}923 + 0{\cdot}199\,[1 - \sin(\pi\alpha/2\alpha')]^4}{\cos(\pi\alpha/2\alpha')}, \tag{5}$$

$$F(\alpha/\alpha') = \sqrt{\frac{2\alpha'}{\pi\alpha} \tan\left(\frac{\pi\alpha}{2\alpha'}\right)} \frac{0{\cdot}752 + 2{\cdot}02\,(\alpha/\alpha') + 0{\cdot}37\,[1 - \sin(\pi\alpha/2\alpha')]^3}{\cos(\pi\alpha/2\alpha')} \tag{6}$$

and

$$\alpha' = \sqrt{D^2 - (2w)^2}. \tag{7}$$

The additional deflection $\hat{u}_i$, due to the crack is given by [19]

$$\hat{u}_i = \frac{\partial}{\partial Q_i}\left[\int J(\alpha)\,\mathrm{d}\alpha\right], \tag{8}$$

where the strain energy density function is given by

$$J(\alpha) = \frac{1}{E}(K^I_{Q_\xi} + K^I_{Q_\eta} + K^I_{Q_u})^2 \tag{9}$$

It may be noted that owing to pure bending assumption, the effect of shear deformation is not taken into account. Also since torsional effects are not considered, cracking in modes II and III involving shear stresses is not present.

The flexibility due to crack is defined as

$$g_i = \frac{\partial \hat{u}_i}{\partial Q_i}. \tag{10}$$

By adding flexibility of uncracked shaft to additional flexibility due to crack we obtain the following flexibility coefficients:

$$g_u = \frac{L}{AE} + \iint \frac{32}{E\pi D^4} \alpha F'(\alpha/\alpha')^2\,\mathrm{d}\alpha\,\mathrm{d}w,$$

$$g_\xi = \frac{L^3}{48EI} + \iint \frac{128L^2\alpha'^2\alpha}{E\pi D^8} F(\alpha/\alpha')^2\,\mathrm{d}\alpha\,\mathrm{d}w,$$

$$g_\eta = \frac{L^3}{48EI} + \iint \frac{512L^2w^2\alpha}{E\pi D^8} F'(\alpha/\alpha')^2\,\mathrm{d}\alpha\,\mathrm{d}w,$$

$$g_{\xi\eta} = g_{\eta\xi} = \iint \frac{256L^2\alpha' w}{E\pi D^8}\alpha F(\alpha/\alpha')F'(\alpha/\alpha')\,\mathrm{d}\alpha\,\mathrm{d}w,$$

$$g_{\xi u} = g_{u\xi} = \iint \frac{64L\alpha'}{E\pi D^6}\alpha F(\alpha/\alpha')F'(\alpha/\alpha')\,\mathrm{d}\alpha\,\mathrm{d}w,$$

$$g_{\eta u} = g_{u\eta} = \iint \frac{128Lw\alpha}{E\pi D^6}F'(\alpha/\alpha')^2\,\mathrm{d}\alpha\,\mathrm{d}w. \tag{11}$$

By inverting the flexibility matrix, corresponding stiffness values are obtained. Thus,

$$\begin{bmatrix} \mathbf{k}_{\xi} & \mathbf{k}_{\xi\eta} & \mathbf{k}_{\xi\mathbf{u}} \\ \mathbf{k}_{\eta\xi} & \mathbf{k}_{\eta} & \mathbf{k}_{\eta\mathbf{u}} \\ \mathbf{k}_{\mathbf{u}\xi} & \mathbf{k}_{\mathbf{u}\eta} & \mathbf{k}_{\mathbf{u}} \end{bmatrix} = \begin{bmatrix} \mathbf{g}_{\xi} & \mathbf{g}_{\xi\eta} & \mathbf{g}_{\xi\mathbf{u}} \\ \mathbf{g}_{\eta\xi} & \mathbf{g}_{\eta} & \mathbf{g}_{\eta\mathbf{u}} \\ \mathbf{g}_{\mathbf{u}\xi} & \mathbf{g}_{\mathbf{u}\eta} & \mathbf{g}_{\mathbf{u}} \end{bmatrix}^{-1}. \tag{12}$$

However, it should be noted that the limits of integration in the expression of flexibility coefficients mentioned above depend on the amount of crack opening [6, 17]. This can be established from the sign of the total SIF (equation (2)) along the crack edge. Integration is to be performed only for the open part of the crack.

Equations of motion (1) can be non-dimensionalized using the following non-dimensional parameters.

$$\bar{\xi} = \xi/\delta_{st}, \quad \bar{\eta} = \eta/\partial_{st}, \quad \bar{u} = u/\partial_{st},$$

$$\zeta = \frac{c}{2\sqrt{k_0 m}}, \quad \tau = \omega t, \; e = \varepsilon/\delta_{st}, \; \bar{a} = a/D,$$

$$r_0 = \omega_0/\omega, \quad r_{\xi} = \omega_{\xi}/\omega, \quad r_{\eta} = \omega_{\eta}/\omega, \quad r_u = \omega_u/\omega, \; r_{unb} = \omega/\omega_0,$$

$$r_{\xi u} = \omega_{\xi u}/\omega, \quad r_{u\xi} = \omega_{u\xi}/\omega, \quad r_{\eta u} = \omega_{\eta u}/\omega, \quad r_{u\eta} = \omega_{u\eta}/\omega, \quad r_{\xi\eta} = \omega_{\xi\eta}/\omega, \quad r_{\eta\xi} = \omega_{\eta\xi}/\omega,$$

where

$$\delta_{st} = mg/k_0, \quad \omega_0 = \sqrt{\frac{k_0}{m}}, \quad \omega_{\xi} = \sqrt{\frac{k_{\xi}}{m}}, \quad \omega_{\eta} = \sqrt{\frac{k_{\eta}}{m}}, \quad \omega_u = \sqrt{\frac{k_u}{m}},$$

$$\omega_{\xi u} = \sqrt{\frac{k_{\xi u}}{m}}, \quad \omega_{u\xi} = \sqrt{\frac{k_{u\xi}}{m}}, \quad \omega_{\eta u} = \sqrt{\frac{k_{\eta u}}{m}}, \quad \omega_{u\eta} = \sqrt{\frac{k_{u\eta}}{m}}, \quad \omega_{\xi\eta} = \sqrt{\frac{k_{\xi\eta}}{m}}, \quad \omega_{\eta\xi} = \sqrt{\frac{k_{\eta\xi}}{m}}. \tag{13}$$

Here, $k_0$ is the stiffness of the shaft without crack. Equations of motion in non-dimensional form are:

$$\ddot{\bar{\xi}} + 2\zeta r_0\dot{\bar{\xi}} - 2\dot{\bar{\eta}} + (r_{\xi}^2 - 1)\bar{\xi} + (r_{\xi\eta}^2 - 2\zeta r_0)\bar{\eta} + r_{\xi u}^2\bar{u} = e\cos\beta - r_0^2\cos\tau,$$

$$\ddot{\bar{\eta}} + 2\zeta r_0\dot{\bar{\eta}} - 2\dot{\bar{\xi}} + (r_{\eta}^2 - 1)\bar{\eta} + (r_{\eta\xi}^2 + 2\zeta r_0)\bar{\xi} + r_{\eta u}^2\bar{u} = e\sin\beta + r_0^2\sin\tau,$$

$$\ddot{\bar{u}} + 2\zeta r_0\dot{\bar{u}} + r_{u\xi}^2\bar{\xi} + r_{u\eta}^2\bar{\eta} + r_u^2\bar{u} = 0. \tag{14}$$

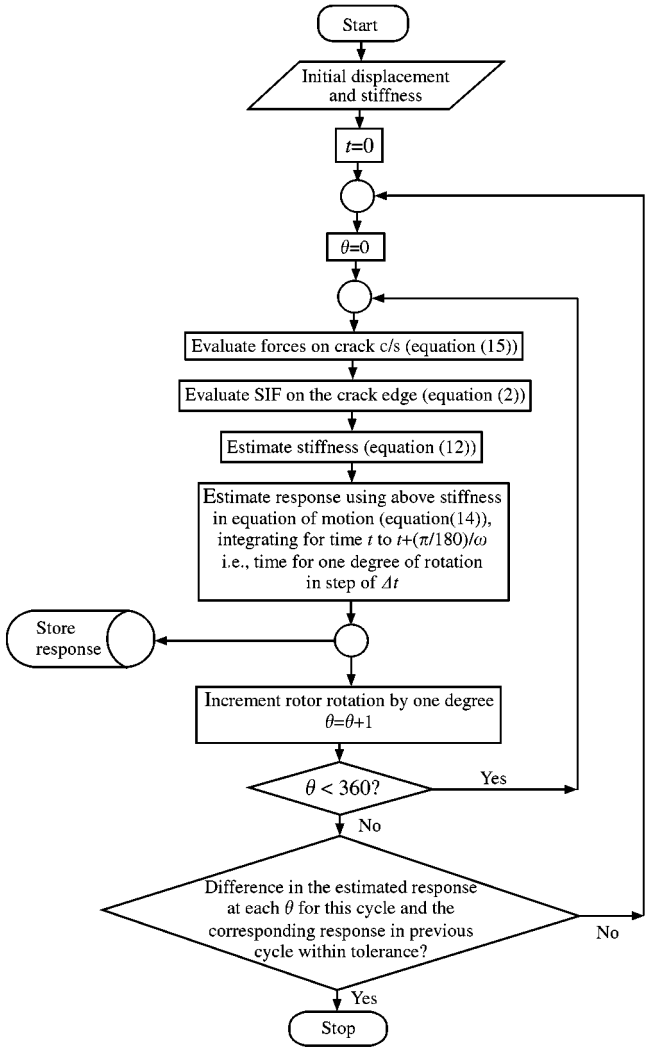


Figure 4. Flowchart showing the procedure of solution of equations of motion.

The solution process for solving the above equations of motion is iterative and is detailed in the flowchart (Figure 4). The initial displacement is assumed to be equal to the static deflection of the rotor and initial stiffnesses correspond to that of an uncracked rotor. Using these initial displacements and stiffnesses, the program evaluates forces ($Q_\xi$, $Q_\eta$ and $Q_u$) on the crack cross-section with the help of the following equations:

$$Q_\xi = k_\xi \xi + k_{\xi\eta}\eta + k_{\xi u}u,$$

$$Q_\eta = k_{\eta\xi}\xi + k_\eta \eta + k_{\eta u}u,$$

$$Q_u = k_{u\xi}\xi + k_{u\eta}\eta + k_u u. \tag{15}$$

Then using these forces, SIF at 50 points across the crack edge is evaluated using equation (2). Positive SIF values indicate the amount of open part of the crack. This in turn

decides the limits of integration for equation (11) since only the open part of the crack is accounted for in finding the additional flexibility due to crack. The calculated flexibility values give stiffnesses using equation (12). Then, equation (14) is integrated using fourth order Runge–Kutta procedure using initial assumed response and stiffnesses evaluated. A program in MATLAB (version 5.3) is written to implement the solution procedure detailed in Figure 4. Stiffnesses are assumed to be constant for one degree of rotation ($\pi/180$ rad), for which the integration of equation (14) is carried out with a sufficiently small time step ($\Delta t = 0{\cdot}00001445$ s) for an accurate solution. The response obtained at the end of one degree of rotation is stored and again used to re-evaluate forces using equation (15). These forces are used to evaluate SIF and eventually the next set of stiffness values which are used in the equation of motion to obtain the next set of displacements ($\xi$, $\eta$ and $u$). Thus, response is used to evaluate stiffnesses which in turn give the next set of responses. To attain a steady state, the iterative procedure is repeated till the response set for one full rotation is converged. The tolerance for convergence of response is taken to be of the order of 0·1%. After the initial transients in the response die within the first few rotor rotations, steady state stabilized solution is obtained.

## 3. RESPONSE OF THE ROTOR WITHOUT EXTERNAL EXCITATION

Steady state response of cracked rotor without any external excitation is first investigated using equation (14). A simply supported shaft of diameter $D = 0{\cdot}015$ m and length $L = 0{\cdot}7$ m with a centrally situated disc of mass $m = 1$ kg is considered. The crack is assumed to be located at mid span. Unbalance with $e = 0{\cdot}1$ and damping ratio $\zeta = 0.01$ are used in all the simulations. The following initial conditions corresponding to static deflection are used.

$$\bar{\xi}(0) = -1, \bar{\eta}(0) = 0, \bar{u}(0) = 0 \quad \text{and} \quad \dot{\bar{\xi}}(0) = 0, \dot{\bar{\eta}}(0) = 0, \dot{\bar{u}}(0) = 0. \tag{16}$$

For $r_{unb} = 0{\cdot}5$ ($r_{unb} = \omega/\omega_0$), the lateral and longitudinal vibration responses are shown in Figures 5 and 6. The responses shown are after several rotations of rotor so as to let the initial transients die. The response shown in these figures is a plot of steady state dimensionless rotor displacement ($\bar{y}$ and $\bar{u}$, respectively) in stationary co-ordinates versus dimensionless time ($\tau$). Figure 5(a) shows rotor displacement in the vertical direction for one complete rotation. The response clearly indicates first and second harmonic ($1\times$ and $2\times$) components of rotational frequency. In axial vibration response (Figure 5(b)) also, the $1\times$ and $2\times$ components along with fundamental natural frequency of axial vibration are

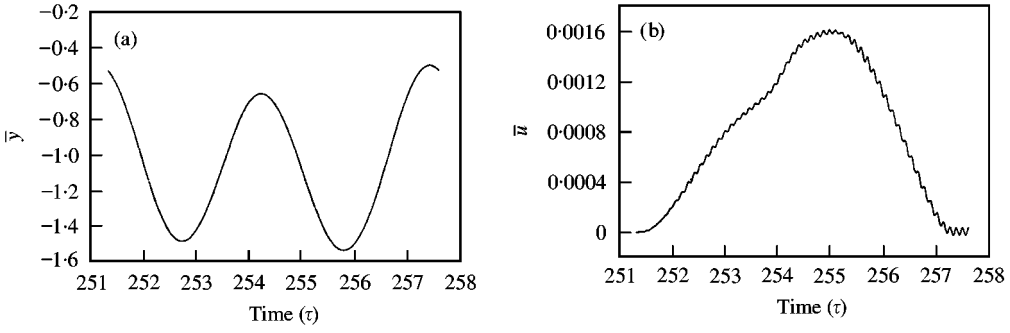


Figure 5. Steady state time domain response of cracked rotor for $\bar{a} = 0{\cdot}4$ and $r_{unb} = 0{\cdot}5$. (a) vertical; (b) axial response.

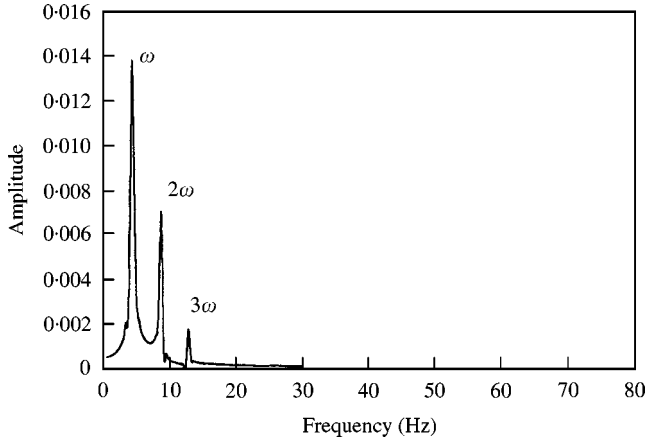


Figure 6. Frequency spectrum of rotor vibration (vertical) of cracked rotor without external axial impulses.

evident. This was also confirmed from the spectrum (not shown here) of the time domain response of Figure 5(b). An extremely weak component at the axial natural frequency (1150 Hz) was found to be present in the spectrum, which corresponds to the ripples in the time domain response of Figure 5(b). Thus in axial vibration response, lateral excitation frequencies coexist with axial natural frequency. However, the level of axial vibration is extremely small. Therefore, in practical terms, it is difficult to detect coupling between lateral and axial vibrations from response measured in the axial direction. The measurable vibrations are in the lateral direction, but contain only lateral excitation frequencies ($1\times$, $2\times$, etc.). Coupling of lateral and axial vibrations is not evident even for a relatively deeper crack ($\bar{a} = 0{\cdot}4$ in this case). The axial vibration frequency component could not be clearly observed in lateral vibration response (Figure 5(a)) due to its high frequency (1150 Hz) and very low amplitude. In fact, the response in the lateral direction is quite similar to the one obtained without considering the coupling of lateral and longitudinal vibrations [6].

In view of the above, it is decided to provide single and multiple axial impulse excitation per rotation to the rotor, which is expected to magnify the lateral–longitudinal vibration coupling effects.

## 4. RESPONSE OF THE ROTOR TO AXIAL IMPULSES

In this case, the initial displacements and velocities corresponding to all the three directions in the equations of motion are taken to be equal to that corresponding to the steady state response found for a given $r_{unb}$ and $\bar{a}$ as discussed in the previous section. To apply the axial impulse in theoretical simulation, the axial velocity at that instant is decreased by $\Delta\dot{\bar{u}} = 800$. For single axial impulse per rotation, the axial velocity is decreased when the rotor is in reference position i.e., $\theta = 0^\circ$, whereas for multiple impulses, $\Delta\dot{\bar{u}}$ is implemented after every $360/i$ degree of rotation, $i$ being the number of impulses per rotation.

A cracked rotor with crack depth ratio $\bar{a} = 0{\cdot}2$ is analyzed for $r_{unb} = 0{\cdot}1$ without subjecting it to axial impulse excitation. The corresponding frequency spectrum (Figure 6) shows rotational frequency ($1\times$) and its harmonics ($2\times$, $3\times$) with decreasing amplitude. To

analyze transient response due to the application of an impulse, an uncracked rotor is subjected to only a single impulse applied at $\tau = 6{\cdot}28$ (at the end of the first rotation). Due to the absence of coupling, the effect of axial impulse is not seen in the response (Figure 7). However, when a cracked rotor ($\bar{a} = 0{\cdot}2$) is subjected to a similar single impulse (at $\tau = 6{\cdot}28$), the transient response (Figure 8) is clearly quite different compared to the uncracked rotor case. The response due to this solitary impulse obviously dies after few rotations since the impulse is not repeated again. The high-frequency vibrations are obvious in the transient response just after the application of impulse. A close view of the time domain response shown in Figure 8(a) reveals a $10\omega$ frequency component (which matches with the bending natural frequency $\omega_0$ of the rotor). In order to assess the effect of application of single impulse (not single impulse per rotation) on the rotor's response, the FFT of the transient response (from $\tau = 6{\cdot}28$ to $44{\cdot}26$) is obtained (Figure 8(b)). This spectrum shows the prominent presence of bending natural frequency along with the rotational frequency.

The time domain response for cracked rotor does not centre around $\bar{y} = -1$ as shown in Figure 8(a). When the rotor passes through $\theta = 180^\circ$ the crack opens fully and consequently, the response $\bar{y}$ dips from $\bar{y} = -0{\cdot}999$ to $-1{\cdot}04$ due to the increased flexibility of the rotor. The response is effectively centred around $\bar{y} = -1{\cdot}002$. In the

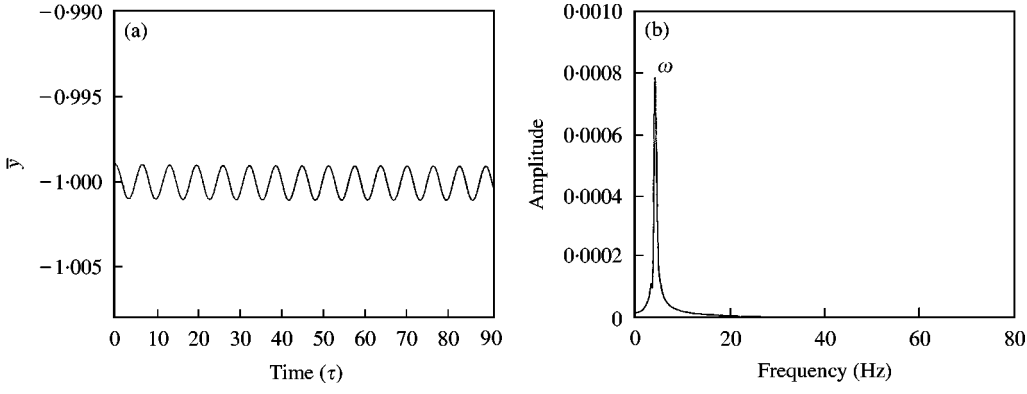


Figure 7. Response of an uncracked rotor to a single impulse applied at $\tau = 6{\cdot}28$, $r_{unb} = 0{\cdot}1$ (a) time domain; (b) frequency domain response.

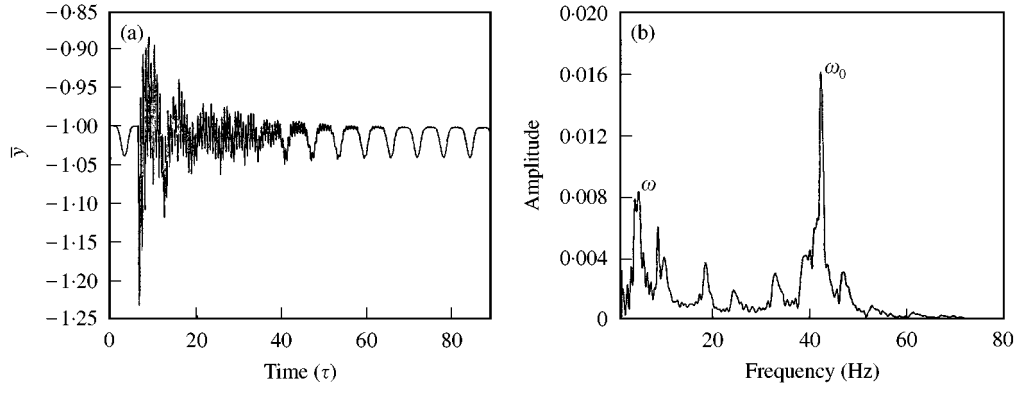


Figure 8. Response of a cracked rotor to a single impulse applied at $\tau = 6{\cdot}28$. $\bar{a} = 0{\cdot}2$, $r_{unb} = 0{\cdot}1$. (a) time domain; (b) frequency domain response.

uncracked rotor, the response fluctuates from $-0{\cdot}999$ to $-1{\cdot}001$, as shown in Figure 7(a) and thus is centred around $\bar{y} = -1$.

When the same rotor is subjected to a single impulse per rotation (periodic impulse excitation), several harmonics are seen in the frequency spectrum (Figure 9(a)), the prominent being the rotor bending natural frequency (42·7 Hz). This is because when single impulse per rotation is applied, the excitation frequencies in the axial direction include rotor running frequency and its higher harmonics. One of the higher harmonics, because of coupling between axial–bending vibrations in a cracked rotor, excites resonant bending vibrations leading to the presence of bending natural frequency in the spectrum. The frequency spectrum of lateral horizontal rotor vibration (Figure 9(b)) is similar. However, the amplitude of the bending natural frequency component is more than that in case of vertical vibration. The presence of bending natural frequency in the spectrum is observed even when the rotor with a minute crack of $\bar{a} = 0{\cdot}01$ is subjected to an axial impulse (Figure 10) although the amplitude of the harmonic is very feeble.

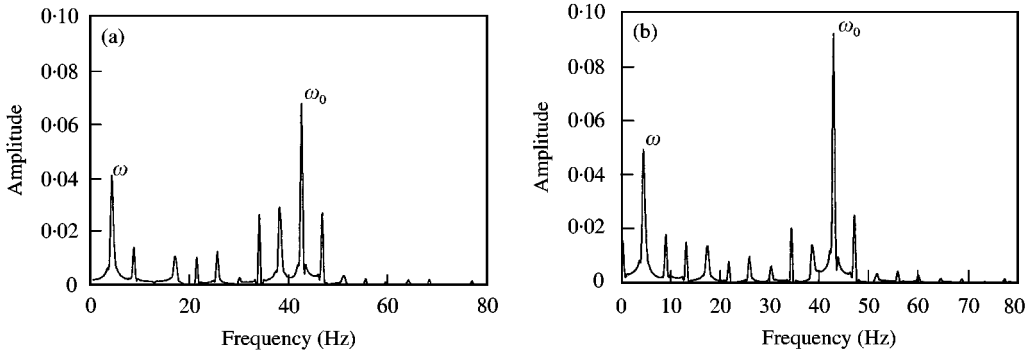


Figure 9. Frequency spectrum of rotor vibration due to single impulse per rotation. (a) vertical; (b) horizontal. $\bar{a} = 0{\cdot}2$, $r_{unb} = 0{\cdot}1$.

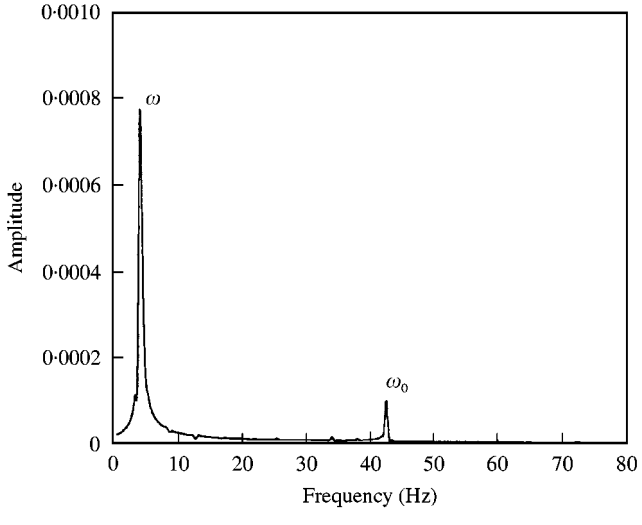


Figure 10. Frequency spectrum of rotor vibration (vertical) of cracked rotor with single impulse per rotation. $\bar{a} = 0{\cdot}01$, $r_{unb} = 0{\cdot}1$.

Next, instead of a single impulse, several impulses are applied per rotation. Rotational speed is kept the same as $r_{unb} = 0{\cdot}1$. Figure 11(a) shows the frequency spectrum of cracked rotor ($\bar{a} = 0{\cdot}2$) vibration (vertical) when the rotor is subjected to four impulses per rotation, the impulse excitation frequency being $\omega_I = 4\omega$. The excitation frequencies in the spectrum of this case are the rotor running frequency $\omega$ (unbalance excitation), the impulse excitation frequency $\omega_I$, as well as its harmonics ($2\omega_I$, $3\omega_I$, etc.). The axial excitation with $4\times$ frequency ($\omega_I$) and its harmonics ($2\omega_I$, $3\omega_I$, etc.) interact with unbalance excitation frequency ($\omega$) to produce sum and difference frequencies $n\omega_I + \omega$ and $n\omega_I - \omega$. This is because the rotor vibration with high-frequency $n\omega_I$ is modulated by a low unbalance excitation frequency $\omega$. The spectrum hence shows the combination harmonics such as $\omega_I + \omega$, $\omega_I - \omega$, $2\omega_I + \omega$, $2\omega_I - \omega$ and so on. The bending natural frequency $\omega_0$ is also prominently seen in the spectrum although neither $\omega_I$ nor any of its higher harmonics matches with $\omega_0$. This is because another lateral vibration frequency component $2\omega$, which exists owing to non-linearity due to crack, also modulates $n\omega_I$, thus giving rise to the presence of $n\omega_I \pm 2\omega$ components in the spectra. The component $2\omega_I + 2\omega$ being equal to $\omega_0$, resonance condition is effected and hence the presence of bending natural frequency in the spectrum. In case of horizontal vibration, the spectrum (Figure 11(b)) is quite similar to that for vertical vibrations, except that the amplitude of bending natural frequency is almost double of that of vertical vibration.

The axial excitation frequency ($\omega_I$) component is small in some of the lateral vibration spectra as shown in Figures 11(a) and 11(b). This is indicative of weak coupling between axial and bending vibrations in a cracked shaft. $\omega_I$ frequency component does appear distinctly in lateral vibration spectrum when the resonating conditions are affected ($\omega_I$ matching with $\omega_0$) as shown in Figure 12. The presence of axial excitation frequency in lateral vibration by way of coupling of vibrations is evident with the presence of sum and difference frequencies ($n\omega_I \pm m\omega$) in lateral vibration spectrum when $n\omega_I$ frequencies interact with rotor running frequency $\omega$ and its harmonics $m\omega$. Collins *et al.* [16] have made similar observations in their study of the effect of axial impulses on cracked rotor. They have reported the presence of sum and difference frequencies only, as in the present case.

The number of impulses are now increased to 10 impulses per rotation so as to match impulse excitation frequency ($\omega_I$) with the bending natural frequency ($\omega_0$). The bending natural frequency ($\omega_0$) component in the frequency spectra is much more prominent along with the sum and difference frequency components. The spectra in this case appear much

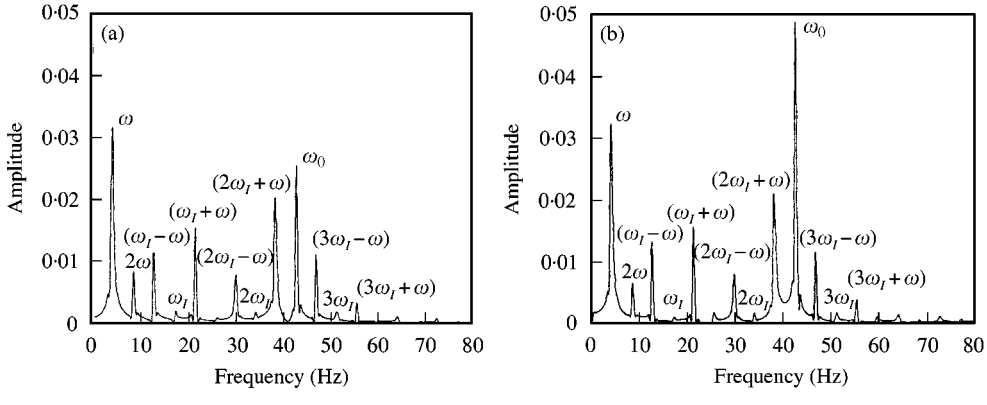


Figure 11. Frequency spectrum of rotor vibration due to four impulses per rotation ($\omega_I = 17$ Hz). (a) vertical; (b) horizontal. $\bar{a} = 0{\cdot}2$ and $r_{unb} = 0{\cdot}1$.

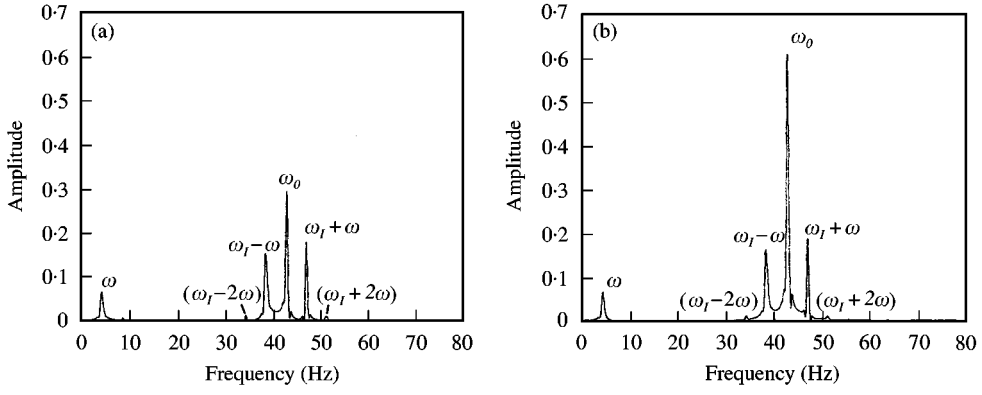


Figure 12. Frequency spectrum of rotor vibration due to 10 impulse per rotation ($\omega_I = 42{\cdot}7$ Hz). (a) vertical; (b) horizontal. $\bar{a} = 0{\cdot}2$, $r_{unb} = 0{\cdot}1$.

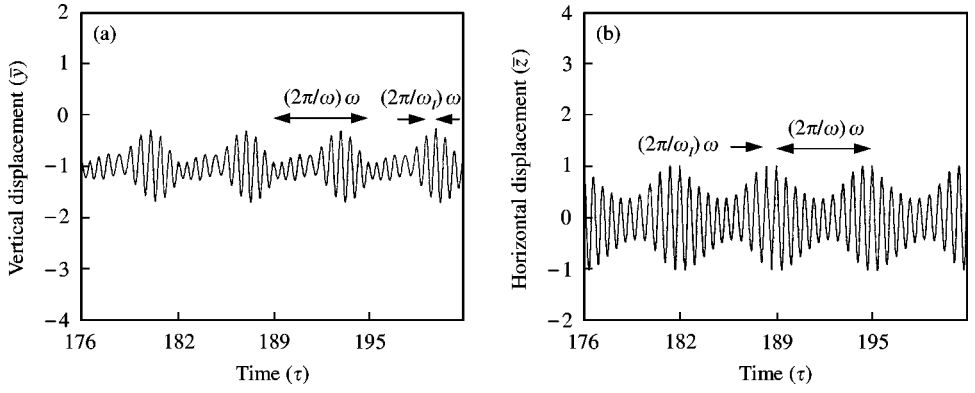


Figure 13. Steady state time domain response showing beating phenomenon. Ten impulses per rotation, $\bar{a} = 0{\cdot}2$, $r_{unb} = 0{\cdot}1$. (a) Vertical; (b) horizontal.

cleaner compared to previous cases (Figures 12(a) and 12(b)). Due to closely spaced side frequencies, there is a clear beating phenomenon observed in the time domain response as shown in Figures 13(a) and 13(b) for vertical and horizontal vibration respectively. In this case of axial excitation, due to coupling mechanism, close sum and difference frequencies exist in lateral vibrations. These frequencies are found to be absent in the case of uncracked rotor under similar excitation conditions. Hence, the beats in the time domain response in the given axial excitation condition can act as a supportive evidence of the presence of crack in the absence of any other mechanism of generation of beats in the rotor response.

The amplitudes of frequency components in the above spectra show considerable increase with increased crack depth ratio. Comparing results of Figures 9 and 14, it can be seen that there is a substantial increase in the amplitude of frequency component $\omega_0$, when $\bar{a}$ is increased from 0·2 to 0·3. Figure 15(a) shows the variation of amplitude of various frequency components with crack depth for the case of single impulse per rotation. The increase in amplitude is non-linear, particularly for bending natural frequency component. Similar variation for the case of 10 impulses per rotation ($\omega_I = \omega_0$) is shown in Figure 15(b).

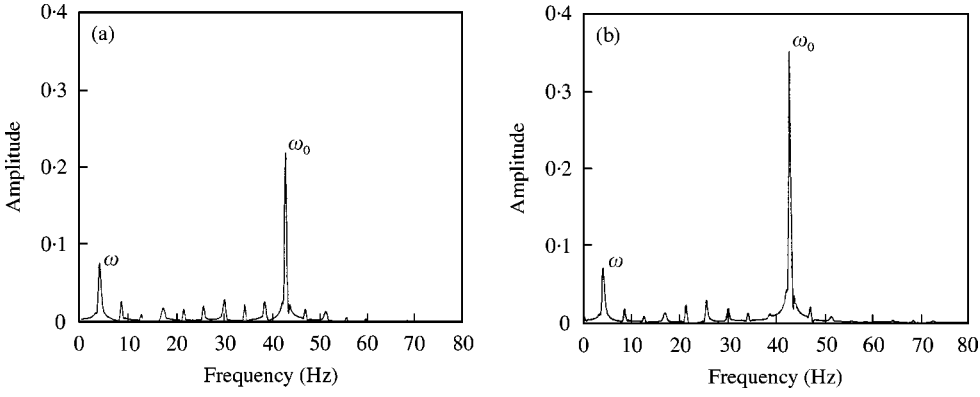


Figure 14. Frequency spectrum of rotor vibration due to single impulse per rotation. $\bar{a} = 0{\cdot}3$, $r_{unb} = 0{\cdot}1$. (a) vertical; (b) horizontal.

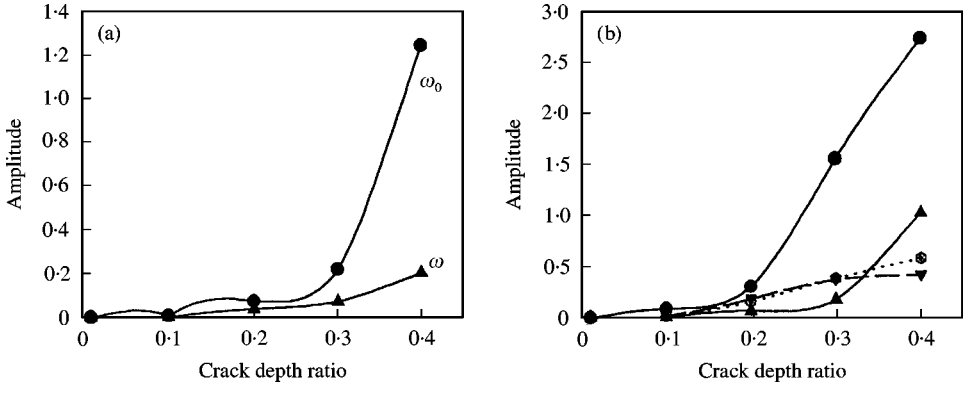


Figure 15. Variation of amplitude of frequency components with crack depth ratio. (a) Single impulse per rotation; (b) 10 impulses per rotation: —▲—, $\omega$; —●—, $\omega_0$; - -⬢- -, $\omega_I - \omega$; —▼—, $\omega_I + \omega$.

Here the amplitudes of the sum and difference frequencies vary quite linearly, whereas the amplitudes of rotational frequency and bending natural frequency show non-linear increase, the latter being very sensitive to crack depth even at a shallow crack depth of $\bar{a} = 0{\cdot}2$.

Excitation using four and eight impulses per rotation with a different rotor speed is also attempted. Here, the speed ($r_{unb} = 0{\cdot}18$) is not an integer fraction of bending critical speed and does not match with any of the subcritical resonances. The frequency spectra for these two cases are shown in Figures 16(a) and 16(b). Since the rotor speed (7·7 Hz) is not an integer fraction of bending critical speed (42·7 Hz), none of the excitation frequencies in either of the above two cases match with the bending natural frequency of the rotor which is obviously absent in the spectrum. The impulse excitation frequency $\omega_I$ is 30·8 and 61·6 Hz for the case of four impulses per rotation and eight impulses per rotation respectively. The presence of sum and difference frequencies ($n\omega_I + \omega$ and $n\omega_I - \omega$) is clearly seen. In fact in Figure 16(a), $2\omega_I + 2\omega$ and $2\omega_I - 2\omega$ frequencies are present. It is clearly established that in order to have a significant magnitude of $\omega_0$ component in the spectrum, either the impulse excitation frequency $\omega_I$ (Figure 12), or any of its higher harmonics (Figure 9) must match with bending natural frequency $\omega_0$.

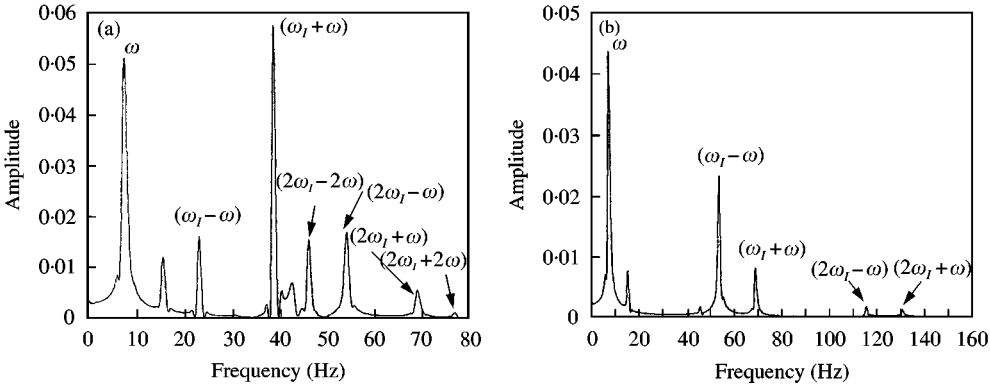


Figure 16. Frequency spectrum of rotor vibration (horizontal) for $\bar{a} = 0{\cdot}2$ and $r_{unb} = 0{\cdot}18$: (a) 4 impulses per rotation ($\omega_I = 30{\cdot}8$ Hz); (b) 8 impulses per rotation ($\omega_I = 61{\cdot}6$ Hz).

## 5. CONCLUDING REMARKS

Steady state response of a cracked Jeffcott rotor subjected to periodic axial impulse excitation is studied. The presence of axial excitation frequencies in the frequency spectrum of lateral vibration indicates the presence of coupling of these lateral and longitudinal vibrations. When a single impulse per rotation is applied to the rotor rotating at a fraction of its bending critical speed, the bending natural frequency appears in the lateral frequency spectrum whereas when more number of impulses are applied, the impulse excitation frequency and its harmonics produce side frequencies in addition to bending natural frequency. When the rotor rotates at a speed that is not a fraction of its bending critical speed, the periodic impulse excitation produces only side frequencies around impulse excitation frequency and its harmonics.

Thus, the presence of bending natural frequency and the side frequencies around impulse excitation frequency and its harmonics in the lateral vibration spectrum, due to coupling of lateral and longitudinal displacements indicates the presence of crack in the rotor. The beats in the time domain response in the given case of axial excitation can act as a supportive evidence of the presence of crack in the absence of any other mechanism of generation of beats in the rotor response.

## REFERENCES

1. J. SCHMIED and E. KRAMER 1984 *Vibrations in Rotating Machinery*, 183–192. London: Institution of Mechanical Engineers Publications. Vibrational behaviour of a rotor with a cross-sectional crack.
2. W. MAYES and W. G. R. DAVIES 1984 *Journal of Vibration, Acoustics, Stress and Reliability in Design* **106**, 139–145. Analysis of the response of the multi-rotor-bearing system containing a transverse crack in a rotor.
3. N. BACHSCHMID, G. DIANA and B. PIZZIGONI 1984 *Vibrations in Rotating Machinery*, 193–198. London: Institution of Mechanical Engineers Publications. The influence of unbalance on cracked rotors.
4. B. GRABOWSKI 1984 *Dynamics of Rotors—Stability and System Identification. CISM Courses & Lectures*, vol. 273, 423–465. New York: Springer. The vibrational behaviour of a rotating shaft containing a transverse crack.

5. IMAM, S. H. AZZARO, R. J. BANKERT and J. SCHEIBEL 1989 *Journal of Vibration, Acoustics, Stress and Reliability in Design* **111**, 241–250. Development of an on-line rotor crack detection and monitoring system.
6. O. S. JUN, H. J. EUN, Y. Y. EARMME and C. W. LEE 1992 *Journal of Sound and Vibration* **155**, 273–290. Modelling and vibration analysis of a simple rotor with a breathing crack.
7. M. C. WU and S. C. HUANG 1998 *Journal of Vibration and Acoustics* **120**, 551–556. In-plane vibration and crack detection of a rotating shaft-disk containing a transverse crack.
8. C. A. PAPADOPOULOS and A. D. DIMAROGONAS 1987 *Ingenieur-Archiv* **57**, 257–266. Coupling of bending and torsional vibration of a cracked Timoshenko shaft.
9. MUSZYNSKA, P. GOLDMAN and D. E. BENTLY 1992 *Vibrations in Rotating Machinery*, 257–262. London: Institution of Mechanical Engineers Conference Publications. Torsional/lateral vibration cross-coupled responses due to shaft anisotropy: a new tool in shaft crack detection.
10. W. M. OSTACHOWICZ and M. KRAWCZUK 1992 *Archives of Applied Mechanics* **62**, 191–201. Coupled torsional and bending vibrations of a rotor with an open crack.
11. C. A. PAPADOPOULOS and A. D. DIMAROGONAS 1987 *Journal of Sound and Vibration* **117**, 81–93. Coupled longitudinal and bending vibrations of a rotating shaft with an open crack.
12. A. PAPADOPOULOS and A. D. DIMAROGONAS 1992 *Journal of Vibration and Acoustics* **114**, 461–467. Coupled vibration of cracked shafts.
13. C. A. PAPADOPOULOS and A. D. DIMAROGONAS 1988 *Journal of Vibration, Acoustics, Stress and Reliability in Design* **110**, 356–359. Stability of cracked rotors in the coupled vibration mode.
14. C. A. PAPADOPOULOS and A. D. DIMAROGONAS 1988 *Journal of Vibration, Acoustics, Stress and Reliability in Design* **110**, 1–8. Coupled longitudinal and bending vibration of a cracked shaft.
15. T. IWATSUBO, S. ARII and A. OKS 1992, *Vibrations in Rotating Machinery*, 275–282. London: Institution of Mechanical Engineers Conference Publications. Detection of a transverse crack in a rotor shaft by adding external force.
16. K. R. COLLINS, R. H. PLAUT and J. WAUER 1991 *Journal of Vibration and Acoustics* **113**, 74–78. Detection of cracks in rotating Timoshenko shafts using axial impulses.
17. O. S. JUN, C. W. LEE, Y. Y. EARMME and H. J. EUN 1992 *Machine Vibration* **1**, 231–235. Analysis of crack growth in a simple rotor with a breathing crack.
18. A. TONDL 1965 *Some Problems of Rotor Dynamics*. Prague: Publishing House of the Crechoslovac Academy of Sciences.
19. H. TADA, P. C. PARIS and G. R. IRWIN 1973 *The Stress Analysis of Crack Handbook*. Hellertown, PA: Del Research Corporation.

## APPENDIX A: NOMENCLATURE

| | |
|---|---|
| $a$ | depth of crack |
| $D$ | diameter of the shaft |
| $\bar{a}$ | crack depth ratio ($a/D$) |
| $L$ | length of the shaft |
| $m$ | mass of the disc |
| $\varepsilon$ | eccentricity of mass of disc from its geometric centre |
| $\delta_{st}$ | static deflection of the rotor |
| $e$ | dimensionless eccentricity ($\varepsilon/\delta_{st}$) |
| $\beta$ | orientation of eccentricity from $\xi$-axis in the direction of shaft rotation |
| $\zeta$ | damping factor |
| $E$ | modulus of elasticity |
| $\theta(t)$ | instantaneous angle of rotation of shaft |
| $y, z$ | dimensional rotor displacement in vertical and horizontal direction respectively |
| $\bar{y}, \bar{z}$ | non-dimensional rotor displacement in vertical and horizontal direction respectively |
| $\xi, \eta$ | dimensional rotor centre displacement in the direction perpendicular to crack edge and in the direction parallel to crack edge respectively |
| $\bar{\xi}, \bar{\eta}$ | non-dimensional rotor centre displacement in the direction perpendicular to crack edge and in the direction parallel to crack edge respectively |
| $u, \bar{u}$ | dimensional and non-dimensional rotor displacement in longitudinal direction |

| | |
|---|---|
| $\tau$ | dimensionless time |
| $\omega$ | rotational frequency |
| $\omega_0$ | natural frequency of lateral vibration of the rotor |
| $\omega_I$ | impulse excitation frequency |
| $r_{unb}$ | dimensionless speed of rotation ($\omega/\omega_0$) |
| $k_0$ | stiffness of the shaft without crack |
| $k_\xi$, $k_\eta$, $k_u$ | direct stiffness of the shaft in $\xi$, $\eta$ and $u$ direction respectively |
| $k_{\xi u}$, $k_{\xi\eta}$, $k_{\eta u}$, $k_{\eta\xi}$, $k_{u\xi}$, $k_{u\eta}$, | cross-coupled stiffnesses |
| $g_\xi$, $g_\eta$, $g_u$ | flexibility in $\xi$, $\eta$ and $u$ direction respectively |
| $g_{\xi u}$, $g_{\xi\eta}$, $g_{\eta u}$, $g_{\eta\xi}$, $g_{u\xi}$, $g_{u\eta}$, | cross-coupled flexibilities |
| $Q_\xi$, $Q_\eta$, $Q_u$ | forces acting on the shaft in $\xi$, $\eta$ and $u$ direction respectively |
| $\sigma_\xi$, $\sigma_\eta$, $\sigma_u$ | stresses acting at a point along the crack edge in $\xi$, $\eta$ and $u$ direction respectively |
| $K^I$ | total stress intensity factor at any point along the crack edge |
| $K^I_{Q\xi}$, $K^I_{Q\eta}$, $K^I_{Qu}$, | stress intensity factor due to forces $Q_\xi$, $Q_\eta$ and $Q_u$ respectively |